TOXICOLOGICAL SCIENCES **90(1)**, 198–207 (2006)
doi:10.1093/toxsci/kfj072
Advance Access publication December 12, 2005

Incorporation of Tissue Reaction Kinetics in a Computational Fluid Dynamics Model for Nasal Extraction of Inhaled Hydrogen Sulfide in Rats

Jeffry D. Schroeter,[1] Julia S. Kimbell, Anna M. Bonner, Kay C. Roberts, Melvin E. Andersen, and David C. Dorman

CIIT Centers for Health Research, 6 Davis Drive, P.O. Box 12137, Research Triangle Park, North Carolina 27709-2137

Received August 16, 2005; accepted December 3, 2005

Rodents exposed to hydrogen sulfide (H_2S) develop olfactory neuronal loss. This lesion has been used by the risk assessment community to develop occupational and environmental exposure standards. A correlation between lesion locations and areas of high H_2S flux to airway walls has been previously demonstrated, but a quantitative dose assessment is needed to extrapolate dose at lesion sites to humans. In this study, nasal extraction (NE) of 10, 80, and 200 ppm H_2S was measured in the isolated upper respiratory tract of anesthetized rats under constant unidirectional inspiratory flow rates of 75, 150, and 300 ml/min. NE was dependent on inspired H_2S concentration and air flow rate: increased NE was observed when H_2S exposure concentrations or inspiratory air flow rates were low. An anatomically accurate, three-dimensional computational fluid dynamics (CFD) model of rat nasal passages was used to predict NE of inhaled H_2S. To account for the observed dependence of NE on H_2S exposure concentration, the boundary condition used at airway walls incorporated first-order and saturable kinetics in nasal tissue to govern mass flux at the air:tissue interface. Since the kinetic parameters cannot be obtained using the CFD model, they were estimated independently by fitting a well-mixed, two-compartment pharmacokinetic (PK) model to the NE data. Predicted extraction values using this PK-motivated CFD approach were in good agreement with the experimental measurements. The CFD model provides estimates of localized H_2S flux to airway walls and can be used to calibrate lesion sites by dose.

Key Words: **hydrogen sulfide; rat; inhalation; pharmacokinetics; computational fluid dynamics; olfactory toxicity; nasal passages.**

Hydrogen sulfide (H_2S) is a naturally occurring and industrially generated gaseous chemical with a characteristic rotten egg odor. In nature, H_2S is produced primarily by the decomposition of organic matter and is found in natural gas, petroleum, and volcanic and sulfur-spring emissions. H_2S emission is also associated with over 70 industrial processes, including artificial fiber synthesis, petroleum and natural gas drilling and refining operations, paper and pulp manufacture, roofing, sewage treatment, and swine containment (ATSDR, 1999).

H_2S is a potent inhibitor of cytochrome oxidase resulting in cellular hypoxia. Target organs include the nervous, cardiovascular, and respiratory systems (ATSDR, 1999). Clinical signs and their severity vary with H_2S concentration and duration of exposure (Beauchamp *et al.*, 1984; Glass, 1990; Reiffenstein *et al.*, 1992). Adverse effects include headaches, nausea, and other symptoms at or near the odor threshold (<1 ppb), and more profound effects such as olfactory paralysis, unconsciousness, and even death can occur in humans following acute exposure to $\geq$500 ppm. Long-term effects of acute H_2S poisoning may include hyposmia, dysosmia, phantosmia, and other signs of olfactory dysfunction (Hirsch and Zavala, 1999; Kilburn, 1997).

Animal studies confirm that the olfactory system is especially sensitive to H_2S inhalation. Subchronic exposure of rats and mice to 30 or 80 ppm H_2S results in olfactory neuron loss and basal cell hyperplasia (Brenneman *et al.*, 2000; Dorman *et al.*, 2004). Cytochrome oxidase inhibition may play a role in H_2S-induced olfactory pathology. Acute high dose H_2S inhalation results in decreased nasal cytochrome oxidase activity and severe mitochondrial swelling in degenerating olfactory neurons within the rat olfactory epithelium (Brenneman *et al.*, 2002; Dorman *et al.*, 2002). Within the olfactory epithelium, sites commonly affected by H_2S border high velocity air streams emanating from the dorsal medial meatus, including the dorsomedial regions of the ethmoid recess, and the tips of the ethmoturbinates (Brenneman *et al.*, 2000).

The location of major airflow routes plays an important role in determining where H_2S-induced olfactory lesions occur since air streams flowing through the nasal passages during breathing influence regional gas uptake (Méry *et al.*, 1994; Morgan *et al.*, 1991). Computational fluid dynamics (CFD) models based on anatomically accurate representations of the geometry of the rat nasal cavity provide a useful tool for investigating gas disposition in flow fields (Kimbell *et al.*, 1993, 2001). A rat CFD model was previously developed to

[1] To whom correspondence should be addressed. Fax: (919) 558-1300. E-mail: jschroeter@ciit.org.

predict nasal regions with low and high flux during H_2S inhalation (Moulin *et al.*, 2002). These simulations assumed that the rate of uptake (flux) at nasal airway walls was directly proportional to the concentration of H_2S near the walls, producing concentration-independent extraction predictions. Due to a lack of information on nasal extraction of H_2S, conditions representing low, medium, and high extraction were simulated. These CFD simulations predicted a correlation between areas of high H_2S flux from airspaces to airway walls with olfactory epithelial responses in the rat nasal cavity regardless of nasal extraction efficiency. However, without measurements of H_2S extraction, the simulations have limited applicability to other species since there is no basis for scaling the parameters used in the CFD model.

The purpose of this study was to measure inhaled H_2S nasal extraction in rats and to subsequently use these data to refine CFD estimates of regional H_2S tissue dose in the rat nasal cavity. Nasal extraction of H_2S was found to be concentration- and air flow rate-dependent. To account for dose-dependent H_2S extraction in the CFD model, the boundary condition relating flux at airway walls to concentration near the walls was modified to include effects of solubility, diffusion, and elimination of H_2S by first-order and saturable kinetics in nasal tissue. Rate constants for tissue reactivity of H_2S are unknown, and they cannot be estimated by directly fitting CFD predictions to nasal extraction data since no automatic optimization methods are currently available to interface with the CFD platform. Therefore, a two-compartment air- and tissue-phase pharmacokinetic (PK) model was developed to simulate H_2S extraction by the rat nasal cavity, where H_2S enters the tissue phase through diffusive flux, and is eliminated in nasal tissue by first-order and saturable pathways. Tissue phase kinetic parameters were estimated by fitting the PK model to the nasal extraction data, and were then implemented in the mass transfer boundary condition in the CFD model. Extraction of H_2S predicted with this PK-motivated CFD model was compared with the experimental uptake measurements to verify the validity of this approach.

MATERIALS AND METHODS

Animals. This study was conducted under federal guidelines for the care and use of laboratory animals (National Research Council, 1996) and was approved by the CIIT Centers for Health Research Institutional Animal Care and Use Committee. A total of 60 male Sprague-Dawley CD (Crl:CD[SD]BR) rats, 8 weeks of age at purchase, were obtained from Charles River Laboratory (Raleigh, NC). Animals were housed on direct bedding (Alpha-Dri, Shepard Specialty Papers, Kalamazoo, MI) in filter-capped cages, and fed certified NIH-07 (Zeigler Brothers, Gardners, PA) and deionized filtered drinking water *ad libitum*. Animal rooms were ventilated with HEPA-filtered air and maintained at 18–26°C with relative humidity of 30–70% on a 12-h dark-light cycle. The general condition of the animals was checked daily. Body weights were recorded at least once weekly. Animals were acclimated for at least two weeks prior to exposure. At the time of use, average body weights (± SEM) were 488 ± 64.7 g.

H_2S nasal extraction measurement. Nasal extraction was measured for constant unidirectional inspiratory flow at rates approximately 50, 100, and 200% of the predicted minute ventilation (150 ml/min) of the adult male CD rat. Nominal H_2S exposure concentrations of 10, 80, and 200 ppm were used. The lowest H_2S exposure concentration used in the study (10 ppm) was the subchronic No-Observed-Adverse-Effect-Level (NOAEL) for nasal olfactory lesions (Brenneman *et al.*, 2000), while acute exposure to the highest H_2S exposure concentration is associated with olfactory neuronal loss (Brenneman *et al.*, 2002). Actual H_2S concentrations were 11.0 ± 0.3, 87.8 ± 3.9, and 206.3 ± 7.0 ppm.

Animals ($n = 5$ rats/exposure concentration/flow rate) were anesthetized with ketamine hydrochloride (Fort Dodge Laboratories, Inc., Fort Dodge, IA) at 100 mg/kg (im or ip), and xylazine (Bayer Corp., Agriculture Division, Animal Health, Shawnee Mission, KS) at 20 mg/kg (im or ip). Anesthetized rats were placed on a heated pad (SnuggleSafe, South Holland, IL) in a supine position, and the trachea was surgically exposed by blunt dissection using methods described by Morris (1999). A 2.5 cm polyethylene endotracheal tube (PE 205, Clay Adams, Parsippany, NJ) was positioned toward the lungs, while a 14-G catheter (4058-20 Jelco, Cincinnati, OH) was inserted into a second tracheal incision so that the catheter tip was positioned near the larynx. The animal's head and nose were placed in an anesthesia nose-only cone (Euthanex Corp., Palmer, PA) to deliver H_2S. Air was drawn through the isolated upper respiratory tract (URT) for 120 min under the desired flow conditions. Body temperature was measured, and anesthesia was monitored and subcutaneously administered as needed every 10–20 min throughout the exposure period. Animals were killed via exsanguination immediately after the end of exposure.

To assess the potential significance of mucociliary and bloodstream effects on H_2S deposition and *in situ* metabolism, nasal extraction was also evaluated in rat cadaver specimens ($n = 3$ rats/exposure concentration) that were treated as described above but killed 2 h prior to H_2S exposure. The air flow rate used for the cadaver exposures was 75 ml/min, or 50% of the predicted minute ventilation for the CD rat.

H_2S vapor generation and characterization. Test atmospheres of H_2S (CAS # 7783-06-4) were generated using gas cylinders containing either 257 (National/Specialty Gases, Research Triangle Park, NC) or 2000 ppm H_2S in air (Holox Gases, Cary, NC). H_2S exposure concentrations were generated by metering H_2S in air from the gas cylinder through a mass flow controller (MKS Instruments, Andover, MA) into a "T" in the dilution air flow where the H_2S was mixed with dilution air to achieve the target concentrations (Fig. 1). The dilution air was drawn from an instrument grade compressed air supply, a portion of which was humidified. The H_2S exposure concentration was controlled by changing the H_2S delivery rate and the dry and humidified air flow rates to achieve the desired concentration and humidity. Total flow rates through the system were maintained at 500 ml/min or greater. The average air temperatures and relative humidity maintained during the 2-h exposures ranged from 22.2–23.4°C and 45–55%, respectively. The exposure portion of the system was contained within a vented portable hood. Vapor-laden, humidified air was drawn continuously through the isolated URT for 120 min at a constant unidirectional flow rate of 75, 150, or 300 ml/min using a rotary vane vacuum pump (GAST Manufacturing, Benton Harbor, MI).

The system used to draw samples consisted of fluorinated ethylene propylene (FEP) or Teflon tubing. Air samples were drawn through a multi-port gas sampling valve connected to a gas chromatograph at a flow rate of 30 ml/min from either the rat anesthesia nose cone or the endotracheal tube using Teflon-based components. Sampling airflow rates were controlled with rotameters and needle valves which were verified using a BIOS DC-1 Flow Calibrator (Bios International Corporation, Pompton Plains, NJ).

H_2S concentrations in the air samples were measured every four minutes using a Hewlett Packard 6890 gas chromatograph (GC) (Agilent Technologies, Palo Alto, CA) equipped with a flame photometric detector. A GS-Q (30 meter × 0.53 μm) column (Alltech, Deerfield, IL) was used at an oven temperature of 80°C. The GC was controlled by Hewlett Packard ChemStation software (Version 04.02) installed on a Hewlett Packard Pavilion Pentium computer. The H_2S peak eluted at 1.2 min after injection onto the column. The GC was

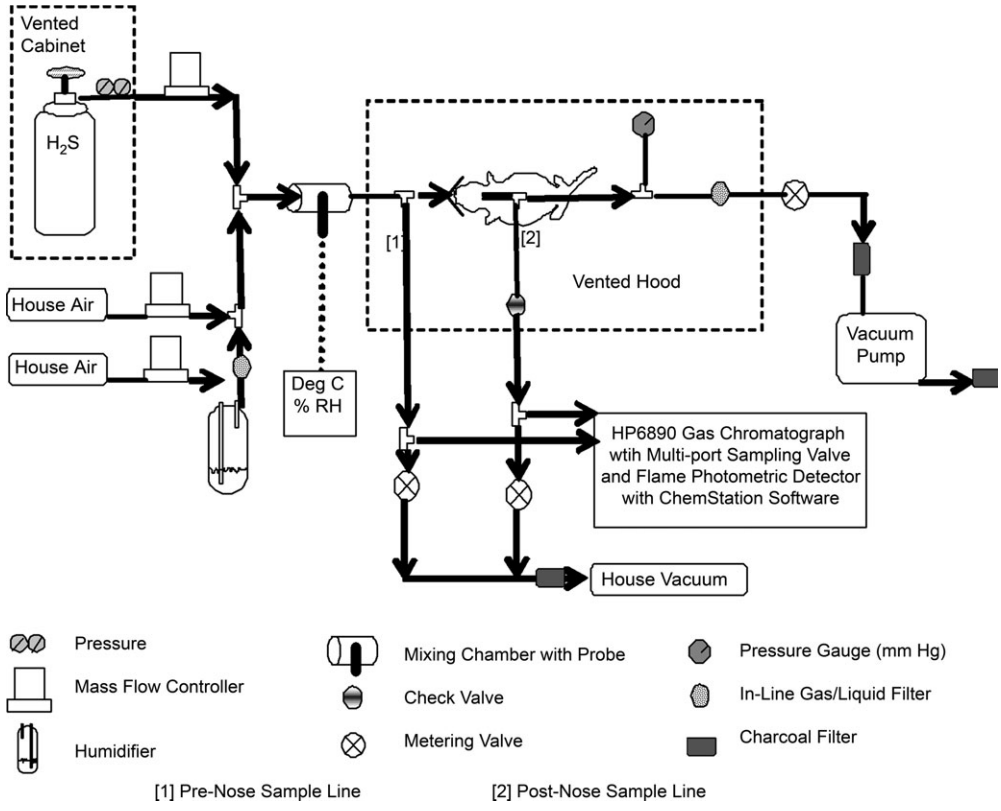

FIG. 1. Schematic diagram of the H_2S exposure system illustrating vapor generation, sampling controls, and placement of the rat in the nose-only chamber.

calibrated using standards made by injecting high purity H_2S (Holox, Ltd., Cary, NC) into Tedlar gas sampling bags (SKC, Inc., Eighty-Four, PA) which were further filled with a measured volume of air to achieve the desired range of concentrations. The air and H_2S mixture were drawn from the bags through the GC gas-sampling valve for analysis. Area counts were converted to concentrations in parts per million of H_2S.

Data analysis. The concentration of H_2S entering the URT (pre-nose) and exiting the URT (post-nose) was measured approximately every 8 min after initiation of flow through the URT through the end of the 120 min H_2S exposure. Inhalation extraction was calculated as [(pre-nose sample – post-nose sample)/pre-nose sample] × 100, and expressed as a percent. The grand mean extraction value was calculated as the overall average of the 15 samples for each animal. Time-averaged extraction data was used to derive parameters for the steady-state CFD model.

To test for the effects of H_2S concentration, air-flow rate, exposure time, and their interactions, experimental data obtained from H_2S-exposed CD rats were analyzed by a 3-factor multivariate analysis of variance with a repeated measures design. A similar analysis for H_2S-exposed live and cadaver specimens was also performed comparing factors of concentration of H_2S, animal status, and exposure time. If the concentration or flow rate effect was significant and the effect was not involved in a significant interaction, Tukey's multiple comparison procedure was used to determine which concentrations and/or flow rates were different. Statistical analyses were performed using SAS Statistical Software (SAS Institute, Inc., Cary, NC). Unless otherwise noted, data are presented as mean ± standard error of the mean (SEM). A probability value of 0.05 was used as the level of significance for all statistical tests.

Development of pharmacokinetic model. A two-compartment pharmacokinetic model was developed assuming well-mixed compartments for both the air and tissue phases of the rat nose (Fig. 2). The air phase component accounts for convective H_2S transport through the nose via inspired air and diffusion to the surrounding tissue. The mass balance differential equation for this phase is:

$$\frac{dX_a}{dt} = Q(C_{in}^{H_2S} - C_{out}^{H_2S}) - k_g S_t \left(C_{out}^{H_2S} - \frac{C_t^{H_2S}}{P_{t:a}} \right), \quad (1)$$

where X_a is the mass of H_2S in the air phase, Q is the inspiratory flow rate, C_{in}, C_{out}, and C_t are the inlet, outlet, and tissue concentrations, respectively, S_t is the surface area of the airway lumen, $P_{t:a}$ is the tissue:air equilibrium partition coefficient, and k_g is the air phase mass transfer coefficient (Table 1). The product of k_g and S_t is the air phase diffusional clearance term (Andersen and Sarangapani, 1999). The value for k_g was derived from methods used in a previous study (Jarabek *et al.*, 2001). This approach involved coronally dividing the CFD model of the F344 rat nose from Kimbell *et al.* (1997) into 12 zones each covering approximately 5 to 10% of the distance from nose to nasopharynx, and calculating the fractional penetration of inhaled gas in each zone. The zones were sequentially made non-absorbing on all tissue anterior to the zone of interest and completely absorbing in the posterior direction to ensure that an adequate concentration boundary layer developed throughout the nose. When a zone was made completely absorbing (i.e., the concentration was set to zero at the air:tissue interface), uptake in that zone did not encounter resistance in the tissue phase, so the total air phase resistance was equal to the gas phase resistance (i.e., contributions from tissue phase transport could be disregarded). Zonal mass transfer coefficients were then calculated and combined into a single air phase mass transfer coefficient for the entire rat nasal cavity.

The first-order ionization reaction of H_2S as it diffuses through tissue is given by:

$$H_2S \rightleftharpoons H^+ + HS^-.$$

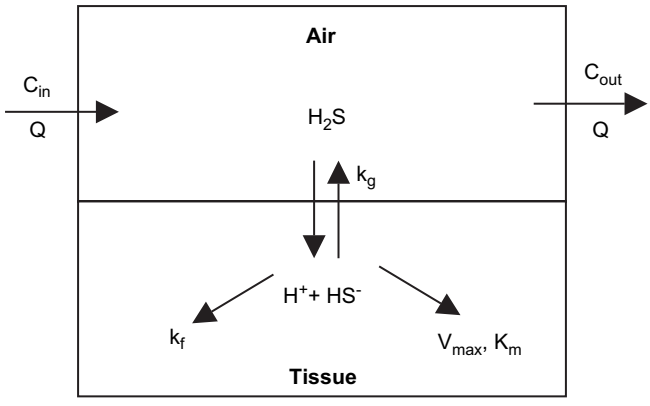

FIG. 2. Schematic of the two-compartment pharmacokinetic model consisting of air and tissue phases representing the rat nasal passages during steady-state inspiration. The air compartment is parameterized by an air phase mass transfer coefficient, k_g. H_2S tissue clearance processes are described by first-order (k_f) and saturable (V_{max} and K_m) pathways.

Elimination of H_2S in nasal tissue was accounted for with first-order and saturable pathways. The mass balance differential equation for the tissue phase is:

$$\frac{dX_t}{dt} = k_g S_t \left(C_{out}^{H_2S} - \frac{C_t^{H_2S}}{P_{t:a}} \right) - k_f V_t C_t^{HS^-} - \frac{V_{\max} \cdot C_t^{HS^-}}{K_m + C_t^{HS^-}}, \quad (2)$$

where X_t is the mass of H_2S in nasal tissue, and V_t is the nasal tissue volume. The first-order rate constant k_f is a combined term reflecting extraction from the nasal cavity arising from systemic delivery and local metabolism; V_{max}, and K_m are the Michaelis-Menten parameters. The equilibrium concentrations of HS^- and H_2S are related by the Henderson-Hasselbach equation:

$$pH = pK_a + \log\left(\frac{[HS^-]}{[H_2S]}\right),$$

where pH is nasal tissue pH, and pK_a is the first-order dissociation constant of H_2S. With a pH of 7.4 (Lantz *et al.*, 2003), and pK_a of 7.04 (ATSDR, 1999), equilibrium concentrations of H_2S and HS^- are related by a factor of 2.29. Therefore, concentrations of HS^- will account for approximately 2/3 of the total tissue sulfur. If the clearance of $[H_2S] + [HS^-]$ had been simulated, then the kinetic parameters would be scaled accordingly. Ongoing studies in our laboratory have shown very slight tissue pH changes occurring in nasal epithelial explant cultures exposed to 400 ppm H_2S for 90 minutes (Roberts, unpublished observation). Therefore, effects of pH change were not considered in the model. Using the previous substitution, the steady-state form of Equations 1 and 2 were solved for nasal extraction (NE), given as percent of mass absorbed in the URT:

$$NE = 100 * \frac{(C_{in}^{H_2S} - C_{out}^{H_2S})}{C_{in}^{H_2S}}.$$

The kinetic parameters k_f, V_{max}, and K_m were obtained by fitting the solution of the PK model to the time-averaged extraction data (nine data points) using a least squares optimization method in Matlab (Mathworks, Inc., Natick, MA).

Development of CFD model. The CFD model developed by Kimbell *et al.* (1997) was used to simulate transport and dosimetry of H_2S in rat nasal passages. This model is an anatomically realistic, 3-D representation of the right nasal passages of a mature 315 g F344 rat that was reconstructed from serial histological cross sections. The computational mesh of the rat nasal cavity consisted of structured hexahedral elements, resulting in approximately 144,000 nodes.

The motion of viscous, incompressible airflow is governed by the Navier-Stokes equations, which in the steady-state form are given by:

$$\rho(u \cdot \nabla u) = -\nabla p + \mu \nabla^2 u \quad (3)$$

$$\nabla \cdot u = 0 \quad (4)$$

where u, p, ρ, and μ are the air velocity, pressure, density, and viscosity, respectively, and ∇ and ∇^2 denote the gradient $(\frac{\partial}{\partial x}, \frac{\partial}{\partial y}, \frac{\partial}{\partial z})$ and Laplacian $(\frac{\partial^2}{\partial x^2} + \frac{\partial^2}{\partial y^2} + \frac{\partial^2}{\partial z^2})$ operators, respectively. The finite element method was used to solve Equations 3 and 4, using the commercial software FIDAP (Fluent, Inc., Lebanon, NH). A no-slip boundary condition was implemented on airway walls, and a uniform velocity profile was defined at the nostril. Previous CFD simulations have predicted that the location of major nasal airflow streams in the inspiratory direction do not change significantly with inspiratory airflow rate (Kimbell *et al.*, 1997). Flow patterns predicted by simulations in which a uniform velocity profile (plug flow) was used at the nostril compared well with dye-streakline visualizations of flow where nostril velocity profiles were presumably not uniform (Kimbell *et al.*, 1993, 1997). Therefore, the plug flow

TABLE 1
Values of H_2S Model Parameters

Parameter	Symbol	Value	Reference
Tissue:air partition coefficient	$P_{t:a}$	2.82	Risk Assessment Information System[a]
Diffusivity in air (cm^2/s)	D_a	0.176	Risk Assessment Information System[a]
Diffusivity in tissue (cm^2/s)	D_t	1.61×10^{-5}	Risk Assessment Information System[a]
Tissue thickness (μm)	L_t	84	Conolly *et al.* (2000)[b]
Tissue surface area of F344 rat (mm^2)	S_t	1851	Kimbell *et al.* (1997)
Tissue volume of F344 rat (mm^3)	V_t	155.5	$V_t = S_t \times L_t$
Nasal tissue pH	pH	7.4	Lantz *et al.* (2003)
First-order dissociation constant	pK_a	7.04	ATSDR (1999)
Air-phase mass transfer coefficient (cm/s)	k_g		Jarabek *et al.* (2001)[c]
Flow rate = 75 ml/min		1.54	
Flow rate = 150 ml/min		2.13	
Flow rate = 300 ml/min		2.94	

[a]Risk Assessment Information System website (http://risk.lsd.ornl.gov) accessed July, 2005.
[b]Value was derived by averaging mucosal thickness from low and high tumor regions.
[c]Values were computed using the methods described in Jarabek *et al.* (2001).

condition was assumed to be a good approximation to the nonuniform velocity profiles from the experimental uptake study, and effects of different inlet velocity profiles on predicted airflow and H_2S flux patterns posterior to the nasal vestibule were assumed to be insignificant. Inter-strain differences in airflow between the CD rats used in the experimental study and the F344 rat used for the CFD model were assumed to be negligible.

Uptake of inhaled gas is governed by convection of inhaled air and molecular diffusion onto airway walls. These processes are simulated by the convection-diffusion equation:

$$u \cdot \nabla C = D_a \nabla^2 C, \tag{5}$$

where u is the air velocity, C is the concentration of inhaled gas, and D_a is the diffusivity of inhaled gas in air. At low concentrations, the presence of gas does not affect airflow behavior, so the airflow velocity in Equation 5 was decoupled from Equations 3–4. The concentration of inhaled H_2S was ascribed at the nostril, and a mass transfer boundary condition relating flux at the airway walls with concentration near the walls was specified on all airway walls.

Implementation of reaction kinetics in nasal tissue. A tissue layer lining the air phase of the CFD model was implemented with one-dimensional diffusion and first-order and saturable metabolism of H_2S (Fig. 3). These tissue phase mass transport processes are governed by the reaction-diffusion equation, which in steady-state form is given by:

$$D_t \frac{d^2C}{dx^2} - k_f \cdot C - \frac{(V_{\max}/V_t) \cdot C}{K_m + C} = 0, \tag{6}$$

where C is the concentration of the dissociated form of H_2S in tissue, D_t is the tissue diffusivity, x is the distance in the tissue phase perpendicular to the air:tissue interface, and k_f, V_{max} and K_m are the rate constants obtained from the solution to the air:tissue pharmacokinetic model (Equations 1–2). Diffusion and reaction in the longitudinal direction were assumed to be negligible. Assuming the diffusion process across the air-tissue interface is in equilibrium, Equation 6 is subject to the boundary conditions:

$$C = P_{t:a} C_{wall} \text{ at } x = 0,$$

$$dC/dx = 0 \text{ at } x = L_t,$$

where nasal tissue is assumed to be of uniform depth L_t, C_{wall} is the concentration of H_2S in air near the airway wall, and systemic clearance of H_2S is included in the first-order rate constant. An analytical solution to Equation 6 exists for the case of first-order reaction. However, an analytical solution is not available for the saturable case considered in this study with the addition of a nonlinear reaction term. Therefore, Equation 6 was solved numerically using a finite difference scheme with Newton's Method.

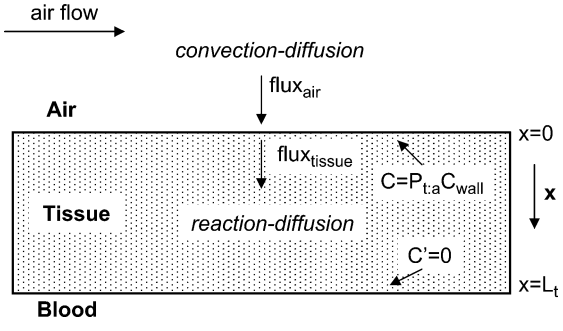

FIG. 3. Schematic of mass transfer at the air:tissue interface of the CFD model. The equilibrium assumption at the air:tissue interface implies that flux onto the interface from the air phase is balanced by flux into tissue ($flux_{air} = flux_{tissue}$), and that H_2S concentrations on either side of the interface are related by a partition coefficient. See text for definitions of C, x, L_t, C_{wall}, and $P_{t:a}$.

The rate of mass transfer across the air:tissue interface in the CFD model serves as a boundary condition for Equation 5, and is given by:

$$flux_{air} = h \cdot C_{wall} \tag{7}$$

where h is the mass transfer coefficient, and $flux_{air}$ is the mass flux across the airway wall. This type of boundary condition is typically used to predict low to moderate extraction of inhaled gases by assigning values of h accordingly.

The equilibrium assumption at the air:tissue interface implies that H_2S flux from the air phase is equal to flux into the tissue layer. This condition of diffusive flux continuity can be written as:

$$D_a \left.\frac{\partial C}{\partial n}\right|_{wall}^{air} = D_t \left.\frac{dC}{dx}\right|_{x=0}^{tissue}, \tag{8}$$

where n is the outward normal vector at the boundary, and x is along the direction of the normal vector. Equations 7 and 8 were used to incorporate tissue diffusion and reaction kinetics from Equation 6 into the mass transfer coefficient that governs nasal extraction of H_2S in the CFD model.

RESULTS

Nasal Extraction Measurements of H_2S

The results of this study indicated that the average nasal extraction (NE) of H_2S was dependent on the concentration of inspired H_2S, the rate of air flow through the URT, and exposure duration. A general decline in NE during the 120-min exposure was observed except at a flow rate of 300 ml/min (Fig. 4). A repeated measures ANOVA revealed time as a significant effect on extraction ($p < 0.001$). Additionally, significant interactions between time and concentration ($p = 0.019$) and time and flow rate ($p < 0.001$) were observed. While average NE of H_2S in cadaver specimens ($n = 3$/concentration) was lower than in live CD rats ($n = 5$/concentration, $p < 0.001$) over the course of the 120-min exposure at a flow rate of 75 ml/min (Fig. 5), the same trends of NE were observed in both subject groups: reduced NE with increasing concentration ($p < 0.001$) and decreasing NE over time ($p < 0.001$). A significant interaction was observed between subject group and concentration ($p = 0.007$), time and concentration ($p = 0.014$), as well as between time and subject group ($p = 0.022$).

Time-averaged NE ranged from 32% for a 10 ppm exposure at 75 ml/min to 7% for a 200 ppm exposure at 300 ml/min (Fig. 6). NE was significantly greater at lower concentrations than at the highest concentration (10 > 80 > 200 ppm) ($p < 0.05$, Tukey's test). Similarly, NE was greater at lower air flow rates than at the highest rate (75 > 150 > 300 ml/min) ($p < 0.05$, Tukey's test). At a flow rate of 150 ml/min (100% of the predicted minute volume), average NE of inspired concentrations of 10 ppm H_2S (26%) was more than double the efficiency of uptake of 200 ppm (10%). Average NE of H_2S during inspiratory flows of 300 ml/min was roughly half the efficiency of uptake during flows of 75 ml/min, regardless of concentration (10 ppm: 20 vs. 32%; 80 ppm: 13 vs. 28%; 200 ppm: 7 vs. 16%).

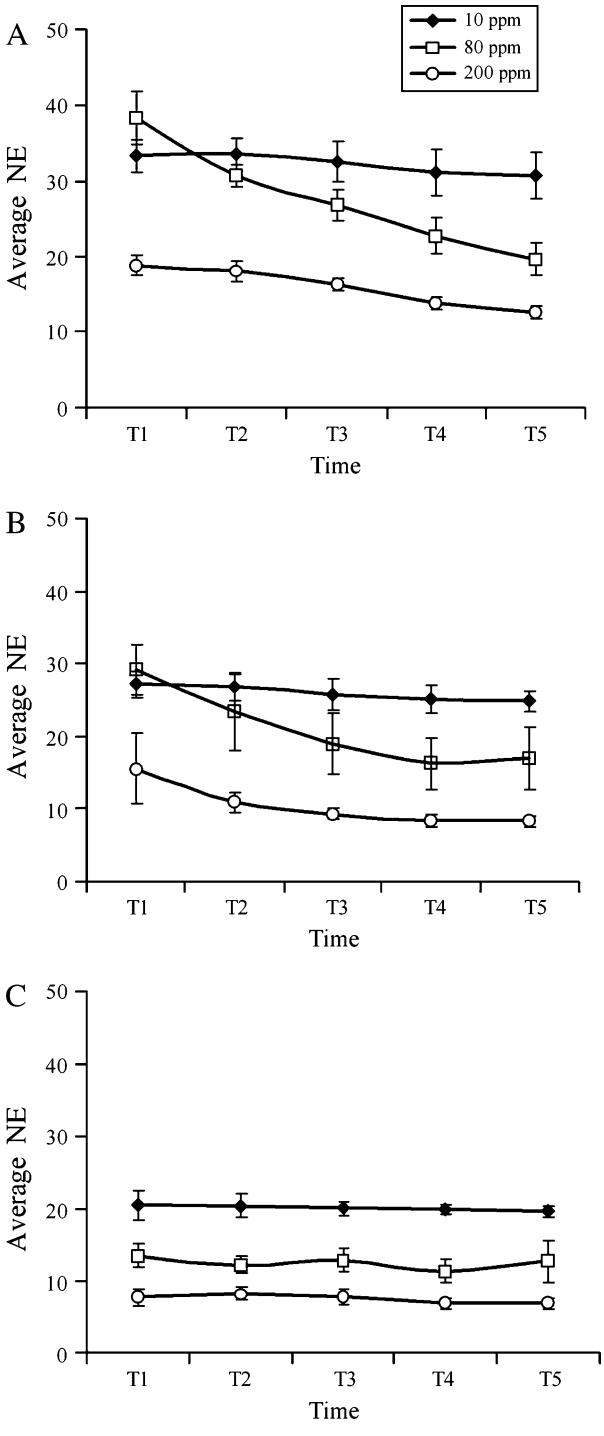

FIG. 4. Mean (± SEM, $n = 5$) H_2S nasal extraction (NE) in the CD rat during the course of a single 2-h exposure: (A) 75 ml/min, (B) 150 ml/min, (C) 300 ml/min. In order to reduce the number of data points for statistical analysis, each successive group of three measurements were averaged, resulting in a single data point per 24 min of exposure, or five data points (T1–T5) per animal.

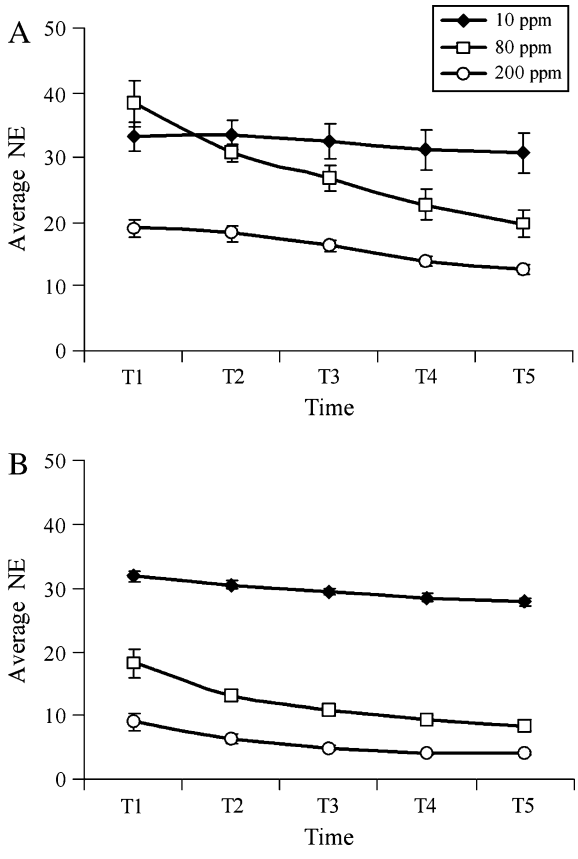

FIG. 5. Mean (± SEM, $n = 5$ live rats, or $n = 3$ cadaver specimens) H_2S nasal extraction (NE) in the CD rat and CD rat cadavers during the course of a single 2-h exposure at a flow rate of 75 ml/min: (A) live rats, (B) cadaver exposures. H_2S concentration, time, and status of the animal significantly affected NE. In order to reduce the number of data points for statistical analysis, each successive group of three measurements were averaged, resulting in a single data point per 24 min of exposure, or five data points (T1–T5) per animal.

Parameter Estimation

A best fit of the solution of the PK model to the NE data was obtained with parameter values of $V_{max} = 183.8$ µmol/min, $K_m = 27.7$ µmol/ml, and $k_f = 5.3$ min^{-1}. NE computed with the PK model using these metabolic parameters at inhalation exposures of 10, 80, and 200 ppm with flow rates of 75, 150, and 300 ml/min show good fits to the experimental data (Fig. 7), indicating that extraction of H_2S can be reasonably simulated with a two-compartment PK model using a combination of first-order and saturable processes in nasal tissue.

CFD Predictions of H_2S Nasal Extraction

To recapitulate the NE data, CFD simulations were conducted at steady-state volumetric inspiratory flow rates of 75, 150, and 300 ml/min (which correspond to Reynolds numbers of 31, 63, and 126 at the nostrils, respectively), with input concentrations of 10, 80, and 200 ppm H_2S. The concentration-dependent mass transfer boundary condition (Equation 7) was

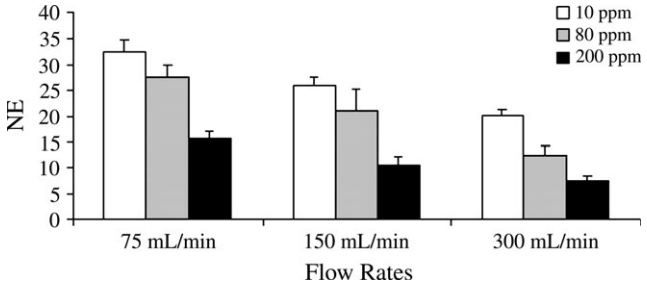

FIG. 6. Time-averaged nasal extraction (NE) of CD rats (mean + SEM, $n = 5$ rats) over the course of a single 2-h inhalation exposure to 10, 80, or 200 ppm H_2S at 50, 100, or 200% of the predicted minute ventilation. Airflow rate and exposure concentration significantly affected NE.

implemented using the kinetic parameters derived from the PK model. The CFD predictions show good overall agreement with the experimental data and the results from the PK model (Fig. 7). The saturable nature of nasal extraction was accurately captured with the CFD model, with the exception of a slight over-prediction of the data at a 200 ppm concentration and 150 ml/min flow rate. At the lowest flow rate, NE predictions ranged from 37% at 10 ppm to 25% at 200 ppm; at a flow rate of 150 ml/min, NE predictions ranged from 19% at 10 ppm to 16% at 80 ppm, with a slight increase to 18% extraction at 200 ppm; and, at a flow rate of 300 ml/min, NE extraction predictions ranged from 10% at 10 ppm to 9% at 200 ppm.

Sensitivity Analysis

Sensitivity analyses of the independent PK and CFD model solutions to the fitted parameters, the tissue:air partition coefficient, and the air phase mass transfer coefficient were performed by varying each parameter by ±5% (Table 2). The sensitivity coefficient was computed by summing the absolute value of the change in NE over the three flow rates, and then taking the maximum value of these sums over the three exposure concentrations and normalizing to the change in parameter value. The PK model was most sensitive to the Michaelis-Menten parameters and the tissue:air partition coefficient, was considerably less sensitive to the first-order rate constant, and was not sensitive to the air phase mass transfer coefficient. The CFD model was very sensitive to all parameters, much more so than the PK model. Sensitivity of the CFD model to the air phase mass transfer coefficient was not performed since this parameter was not explicitly used in CFD simulations.

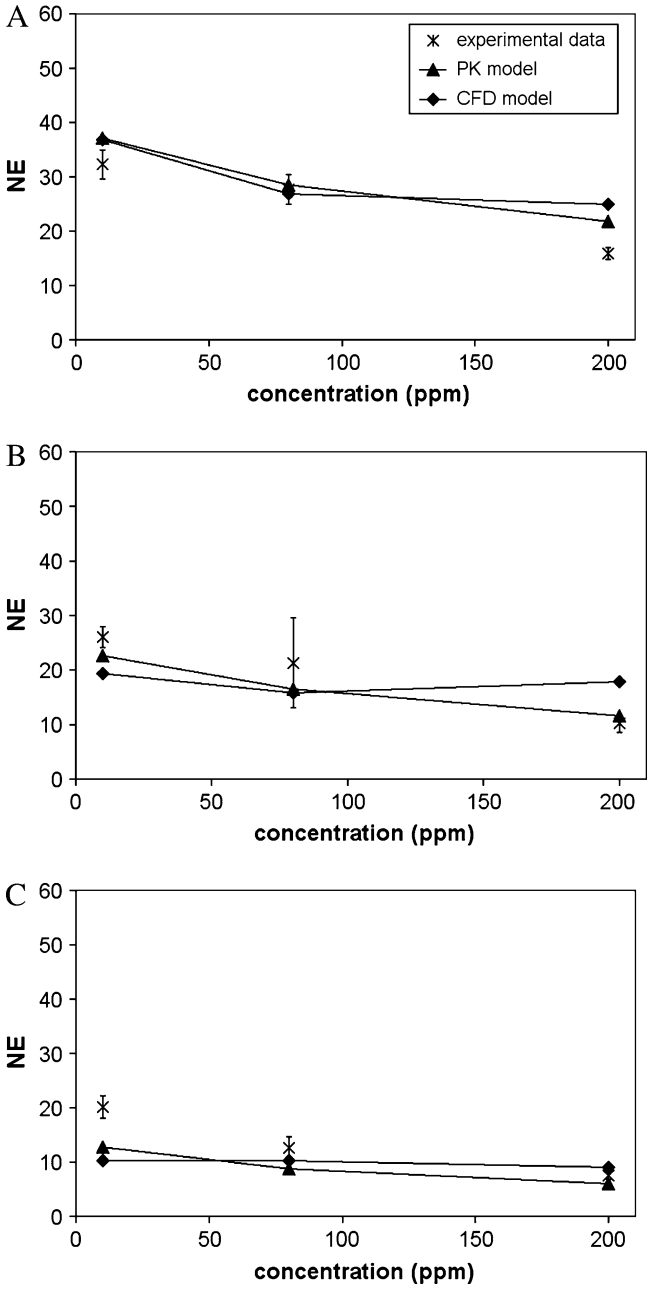

FIG. 7. Predictions of nasal extraction (NE) from the CFD and PK models with mean time-averaged NE data: (A) 75 ml/min; (B) 150 ml/min; (C) 300 ml/min.

DISCUSSION

The results of this study indicated that average NE of H_2S was dependent on concentration of inspired H_2S, rate of air flow through the URT, and exposure duration. At a flow rate analogous to 100% of the predicted minute volume, average NE of inspired concentrations of 10 ppm H_2S was more than double the extraction at 200 ppm. This concentration-dependent behavior observable at all three flow rates indicates that nonlinear, presumably saturable uptake processes are responsible for extraction of H_2S in the rat nasal cavity. Further, an increased ventilation rate for H_2S in the URT was noted to have a profound effect on NE due to the decreased residence time. During inspiratory flows of 300 ml/min, average NE was roughly half the efficiency of uptake observed

TABLE 2
Sensitivity Coefficients for Model Parameters

	Sensitivity coefficient	
Parameter	PK model	CFD model
k_g	0.01	x
$P_{t:a}$	0.49	2.29
V_{max}	0.46	1.98
K_m	0.42	1.48
k_f	0.09	1.82

during flows of 75 ml/min, regardless of H_2S concentration. A decrease of 32 to 20% at 10 ppm, of 28 to 13% at 80 ppm, and 16 to 7% at 200 ppm was observed when the ventilation rate increased from 50% to 200% of the predicted minute volume for CD rats.

CFD simulations conducted with the model previously developed by Moulin *et al.* (2002) could not recapitulate the observed dependence of NE on H_2S exposure concentration due to the constant proportionality factor relating flux with concentration that had been implemented at the boundary (i.e., the value of h in Equation 6 was held constant for each case). Application of this type of boundary condition leads to overall absorption that varies linearly with exposure concentration, which, in turn yields concentration-independent results for NE. Due to a lack of information on H_2S reactivity and solubility, three cases were considered in the study by Moulin and colleagues (2002): low, medium, and high extraction conditions represented by extraction values of 20, 40, and 80%, respectively. The three extraction cases resulted from the imposition of different proportionality constants for each scenario. Even though a good correlation was found between flux and lesion location regardless of extraction value, localized dose computed in this manner is only a qualitative measure since actual H_2S extraction was unknown.

To achieve concentration-dependent uptake simulations with the CFD model, the flux boundary condition developed for this study was expanded from a constant mass-transfer coefficient, as in Equation 6, to one that includes solubility, diffusivity, and chemical reaction kinetics of H_2S in nasal tissue. Incorporation of a nasal lining description into a CFD model to predict uptake of inhaled gases has previously been studied by several other investigators. Keyhani and colleagues (1997) developed a human nasal model where the mass transfer coefficient applied at airway walls included effects of solubility and diffusion in a mucus layer; Scherer and colleagues (1994) used this same model with a first-order reaction term to study uptake of inhaled ozone; and, Cohen Hubal and colleagues (1996) implemented a mucus/tissue layer with diffusion and first-order reaction to predict ozone dosimetry in a rat nasal CFD model. In these studies, a form of the reaction-diffusion equation simulating mass transport in mucus and/or tissue was solved analytically to derive a formula for the air phase mass transfer coefficient used in the boundary condition at the air-mucus interface. A similar approach was undertaken in this study, but with the addition of Michaelis-Menten kinetics in the reaction-diffusion equation to account for the observed concentration dependence of H_2S extraction. An analytical solution was not available with the addition of this nonlinear term, so a standard finite difference scheme was implemented to numerically solve the equation.

By having the mass transfer term implicitly determined by tissue reaction kinetics, extraction was governed by the kinetic parameters k_f, V_{max}, and K_m. No experimental measurements of these kinetic parameters were available, so they were estimated by fitting predicted NE to the time-averaged extraction data measured in this study. Ideally, a parameter estimation would be performed by fitting solutions of the CFD model to the experimental data. However, since extraction behavior was a function of the interplay of three unknown parameters, this approach would be overwhelmingly computationally intensive since there are no automatic optimization routines available to interface with the CFD platform. Therefore, a simple two-compartment PK model with air and tissue phases was developed to estimate the unknown parameters.

The two-compartment PK model simulated the clearance processes of the rat nose while keeping computational requirements and anatomical complexity at a minimum. The air phase was parameterized with a single mass transfer term, and H_2S tissue kinetics were described by first-order and saturable pathways. The metabolic parameters in the PK model were fit to the NE data using a standard least squares optimization algorithm. These parameters were then used in the CFD boundary condition to obtain predicted uptake values in a more anatomically realistic model of rat nasal passages. Incorporation of a tissue phase into the CFD model was required so that the CFD and PK models shared a similar model structure. This novel approach was designed to utilize the advantages of both types of models. The PK model enabled estimation of parameters that could not be computed using only the CFD model, and the coupling of this output with CFD simulations enabled us to generate localized extraction predictions that can be used to calibrate H_2S-induced lesions located in specific sites of the rat nasal passages by dose.

Predictions of nasal extraction using this PK-motivated CFD model adequately captured the saturation of H_2S extraction that was evident in the experimental data (Fig. 7). Predictions from the CFD model at the three flow rates of 75, 150, and 300 ml/min were in good agreement with the output from the PK model and the experimental measurements. The largest discrepancies between CFD predictions and experimental measurements occurred at a 200 ppm exposure with a 75 ml/min flow rate, a 200 ppm exposure with a 150 ml/min flow rate, and at a 10 ppm exposure with a 300 ml/min flow rate. For the first and third cases, the CFD model was in good agreement with the PK model, and both models consistently over- and

under-predicted the experimental data, respectively. For the second case, a significant over-prediction was observed by the CFD model when compared with the PK model and the experimental data. This discrepancy may be attributable to relatively high mass balance errors. For all nine simulations, the average mass-balance error was about 5%, with the highest errors occurring at the lowest flow rate, and error decreasing as extraction decreased. Mass loss was due to both numerical accuracy and flux calculations at the air:tissue interface where the complexity of the shape of the nasal passages leads to some inaccuracy.

Discrepancies should also be expected due to the interfacing of two models with different anatomical realizations. The metabolic parameters were optimized for a well-mixed compartment, which, by design, assumes a constant value of the outlet concentration throughout the compartment, and is unable to describe proximal to distal concentration gradients. Although the use of parameters from well-mixed models in distributed models may theoretically lead to over-predictions at higher extraction values (Andersen and Sarangapani, 1999), the relatively low NE of H_2S measured in this study minimizes this effect.

Diffusive flux at the air-tissue interface of the PK model is described by a mass transfer coefficient, denoted k_g, which is considered a lumped parameter based on average concentrations in well-mixed air and tissue compartments. On the other hand, the CFD model is based on a high degree of anatomical accuracy with the ability to predict localized regions of low and high mass flux throughout the rat nasal cavity. The air and tissue phases of the CFD model are considered distributed parameter models, where mass transport is governed by convection-diffusion and reaction-diffusion processes, respectively, and diffusive flux is governed by Fick's law of diffusion, using respective diffusion coefficients in each phase. The parameter h that relates mass flux on either side of the air-tissue interface in the CFD model is also referred to as a mass transfer coefficient, but in this case it is considered a distributed parameter responsible for characterizing localized concentration differences. Although the term ''mass transfer coefficient'' is used interchangeably in both contexts, differences should be recognized in the exact definitions depending on the type of model being considered. Nevertheless, in both instances the mass transfer coefficient represents a proportionality value between flux and concentration gradient at the air-tissue interface.

To capture extraction and flow dynamics in the nasal cavity more accurately, a more comprehensive PK model could have been used, including additions of a mucus compartment, blood compartment, tissue layers, or separate tissue components based on airflow patterns (Morris, 1993). However, use of these additional compartments would add complexity to the tissue phase of the CFD model, and would also add more unknown parameters to the system. Since a simple two-compartment PK model was considered sufficient to adequately describe H_2S extraction measurements, use of a more elaborate PK model was deemed unnecessary.

There have been numerous modeling efforts with hybrid CFD-PBPK models (e.g., Andersen *et al.*, 1999; Bush *et al.*, 1998; Frederick *et al.*, 1998). In these studies, the CFD model of the rat nasal cavity developed by Kimbell and colleagues (1993, 1997) was used to compute regional air phase mass transfer coefficients using a zero-concentration boundary condition to simulate gas uptake. These compartment-based coefficients were based on major airflow streams and were input into physiologically based pharmacokinetic (PBPK) models to estimate tissue doses in discrete regions of the rat and human nasal cavity. Although these hybrid CFD-PBPK models incorporated flow patterns and mass transfer coefficients from an anatomically accurate CFD model of the rat nasal cavity, tissue doses were computed with a compartmental PBPK model. It has already been established that airflow-driven uptake patterns play an important role in the distribution of H_2S-induced olfactory lesions in rats. Therefore, the level of detail provided by the CFD model used in this study was necessary to obtain estimates of local tissue dose to correlate with nasal olfactory lesions.

Although the exact nature of the interactions governed by the Michaelis-Menten parameters is unknown, concentration-dependent pharmacokinetic behavior is consistent with H_2S interacting with enzymes within the nasal epithelium. Binding of H_2S with cytochrome oxidase is known to occur and results in inhibition of this enzyme (Khan *et al.*, 1990; Nicholls, 1975). Cyanide is another irreversible cytochrome oxidase inhibitor whose kinetic effect is to decrease the concentration of active enzyme within the cell. Other investigators have shown that inhibition of cytochrome oxidase by cyanide displays concentration-dependent behaviors (Pettersen and Cohen, 1993). Cadaver specimens were evaluated in the present study to determine what extent H_2S uptake reflects direct chemical reactivity or other uptake processes that are independent of nasal metabolism or circulatory effects. These studies showed that nonspecific uptake mechanisms likely account for a significant portion of the H_2S that is absorbed by the rat nasal cavity.

In summary, the objectives of this study were (1) to measure NE of H_2S in rats under constant unidirectional flow, (2) to use a simple PK model with the extraction data to estimate unknown kinetic parameters of H_2S, and (3) to incorporate these parameters into a CFD model to refine estimates of regional H_2S tissue dose in the rat nasal cavity. We have demonstrated that a two-compartment PK model is adequate to predict NE of H_2S, and that the parameters derived from this model can successfully be used in an anatomically accurate CFD model of the rat nasal passages. Using this PK-motivated approach, a novel CFD model was developed that entails convection and diffusion in nasal airspace, and mass transport by diffusion and first-order and saturable reaction kinetics in nasal tissue. Since the CFD model is calibrated to the H_2S

extraction data, we are now able to quantitatively predict localized tissue dose in the rat and extrapolate these results by appropriately scaling the kinetic parameters to obtain estimates of risks to human health.

ACKNOWLEDGMENTS

This study was funded in part by a grant from the American Forest and Paper Association (AF&PA) and by the American Chemistry Council. The authors acknowledge the technical assistance of the members of the CIIT animal care, inhalation, and pathology service groups. The authors also thank Matthew Godo and Marc Horner for discussions involving implementation of a saturable boundary condition in FIDAP, and Darin Kalisak for computer programming assistance. We appreciate the comments of Harvey Clewell, Annie Jarabek, and Elizabeth Roberts for their review of the manuscript.

REFERENCES

Agency for Toxic Substances and Disease Registry (ATSDR) (1999). Toxicological Profile for Hydrogen Sulfide, U.S. Department of Commerce, Springfield, VA.

Andersen, M. E., and Sarangapani, R. (1999). Clearance concepts applied to the metabolism of inhaled vapors in tissues lining the nasal cavity. *Inhal. Toxicol.* **11,** 873–897.

Andersen, M. E., Sarangapani, R., Frederick, C. B., and Kimbell, J. S. (1999). Dosimetric adjustment factors for methyl methacrylate derived from a steady-state analysis of a physiologically based clearance-extraction model. *Inhal. Toxicol.* **11,** 899–926.

Beauchamp, R. O., Jr., Bus, J. S., Popp, J. A., Boreiko, C. J., and Andjelkovich, D. A. (1984). A critical review of the literature on hydrogen sulfide toxicity. *Crit. Rev. Toxicol.* **13,** 25–97.

Brenneman, K. A., James, R. A., Gross, E. A., and Dorman, D. C. (2000). Olfactory neuronal loss following subchronic inhalation exposure to low levels of hydrogen sulfide in adult male CD rats. *Toxicol. Pathol.* **28,** 326–333.

Brenneman, K. A., Meleason, D. F., Marshall, M. W., James, R. A., Gross, E. A., Martin, J. T., and Dorman, D. C. (2002). Nasal lesions following acute inhalation exposure of male CD rats to hydrogen sulfide: Reversiblity and the possible role of regional metabolic capacity in lesion distribution. *Toxicol. Pathol.* **30,** 200–208.

Bush, M. L., Frederick, C. B., Kimbell, J. S., and Ultman, J. S. (1998). A CFD-PBPK hybrid model for simulating gas and vapor uptake in the rat nose. *Toxicol. Appl. Pharmacol.* **150,** 133–145.

Cohen Hubal, E. A., Kimbell, J. S., and Fedkiw, P. S. (1996). Incorporation of nasal-lining mass-transfer resistance into a CFD model for prediction of ozone dosimetry in the upper respiratory tract. *Inhal. Toxicol.* **8,** 831–857.

Conolly, R. B., Lilly, P. D., and Kimbell, J. S. (2000). Simulation modeling of the tissue disposition of formaldehyde to predict nasal DNA-protein cross-links in F344 rats, rhesus monkeys, and humans. *Environ. Health Perspect.* **108(Suppl. 5),** 919–924.

Dorman, D. C., Moulin, F. J. M., McManus, B. E., Mahle, K. C., James, R. A., and Struve, M. F. (2002). Cytochrome oxidase inhibition induced by acute hydrogen sulfide inhalation: Correlation with tissue sulfide concentrations in the rat brain, liver, lung, and nasal epithelium. *Toxicol. Sci.* **65,** 18–25.

Dorman, D. C., Struve, M. F., Gross, E. A., and Brenneman, K. A. (2004). Respiratory tract toxicity of inhaled hydrogen sulfide in Fischer-344 Rats, Sprague Dawley Rats, and B6C3F1 mice following subchronic (90-day) exposure. *Toxicol. Appl. Pharmacol.* **198,** 29–39.

Frederick, C. B., Bush, M. L., Lomax, L. G., Black, K. A., Finch, L., Kimbell, J. S., Morgan, K. T., Subramaniam, R. P., Morris, J. B., and Ultman, J. S. (1998). Application of a hybrid computational fluid dynamics and physiologically based inhalation model for interspecies dosimetry extrapolation of acidic vapors in the upper airways. *Toxicol. Appl. Pharmacol.* **152,** 211–231.

Glass, D. C. (1990). A review of the health effects of hydrogen sulphide exposure. *Ann. Occup. Hyg.* **34,** 323–327.

Hirsch, A. R., and Zavala, G. (1999). Long term effects on the olfactory system of exposure to hydrogen sulfide. *Occup. Environ. Med.* **56,** 284–287.

Jarabek, A. M., Kimbell, J. S., Schlosser, P. M., Lou, S. R., and Hanna, L. M. (2001). Computational fluid dynamics and mass transport calculations update the inhalation reference concentration methods: rat. *Toxicol. Sci.* **60,** 150.

Keyhani, K., Scherer, P. W., and Mozell, M. M. (1997). A numerical model of nasal odorant transport for the analysis of human olfaction. *J. Theor. Biol.* **186,** 279–301.

Khan, A. A., Schuler, M. M., Prior, M. G., Yong, S., Coppock, R. W., Florence, L. Z., and Lillie, L. E. (1990). Effects of hydrogen sulfide exposure on lung mitochondrial respiratory chain enzymes in rats. *Toxicol. Appl. Pharmacol.* **103,** 482–490.

Kilburn, K. H. (1997). Exposure to reduced sulfur gases impairs neurobehavioral function. *South Med. J.* **90,** 997–1006.

Kimbell, J. S., Godo, M. N., Gross, E. A., Joyner, D. R., Richardson, R. B., and Morgan, K. T. (1997). Computer simulation of inspiratory airflow in all regions of the F344 rat nasal passages. *Toxicol. Appl. Pharmacol.* **145,** 388–398.

Kimbell, J. S., Gross, E. A., Joyner, D. R., Godo, M. N., and Morgan, K. T. (1993). Application of computational fluid dynamics to regional dosimetry of inhaled chemicals in the upper respiratory tract of the rat. *Toxicol. Appl. Pharmacol.* **121,** 253–263.

Kimbell, J. S., Subramaniam, R. P., Gross, E. A., Schlosser, P. M., and Morgan, K. T. (2001). Dosimetry modeling of inhaled formaldehyde: Comparisons of local flux predictions in the rat, monkey, and human nasal passages. *Toxicol. Sci.* **64,** 100–110.

Lantz, R. C., Orozco, J., and Bogdanffy, M. S. (2003). Vinyl acetate decreases intracellular pH in rat nasal epithelial cell. *Toxicol. Sci.* **75,** 423–431.

Méry, S., Gross, E. A., Joyner, D. R., Godo, M., and Morgan, K. T. (1994). Nasal diagrams: A tool for recording the distribution of nasal lesions in rats and mice. *Toxicol. Pathol.* **22,** 353–372.

Morgan, K. T., Kimbell, J. S., Monticello, T. M., Patra, A. L., and Fleishman, A. (1991). Studies of inspiratory airflow patterns in the nasal passages of the F344 rat and rhesus monkey using nasal molds: Relevance to formaldehyde toxicity. *Toxicol. Appl. Pharmacol.* **110,** 223–240.

Morris, J. B. (1999). A method for measuring upper respiratory tract vapor uptake and its applicability to quantitative inhalation risk assessment. *Inhal. Toxicol.* **11,** 943–965.

Morris, J. B., Hassett, D. N., and Blanchard, K. T. (1993). A physiologically based pharmacokinetic model for nasal uptake and metabolism of non-reactive vapors. *Toxicol. Appl. Pharmacol.* **123,** 120–129.

Moulin, F. J.-M., Brenneman, K. A., Kimbell, J. S., and Dorman, D. C. (2002). Predicted regional flux of hydrogen sulfide correlates with distribution of nasal olfactory lesions in rats. *Toxicol. Sci.* **66,** 7–15.

National Research Council. (1996). Guide for the care and use of laboratory animals. Washington, DC: National Academy Press.

Nicholls, P. (1975). The effect of sulphide on cytochrome aa3 isosteric and allosteric shifts of the reduced α-peak. *Biochim. Biophys. Acta* **396,** 24–35.

Pettersen, J. C., and Cohen, S. D. (1993). The effects of cyanide on brain mitochondrial cytochrome oxidase and respiratory activities. *J. Appl. Toxicol.* **13,** 9–14.

Reiffenstein, R. J., Hulbert, W. C., and Roth, S. H. (1992). Toxicology of hydrogen sulfide. *Ann. Rev. Pharmacol. Toxicol.* **32,** 109–134.

Scherer, P. W., Keyhani, K., and Mozell, M. M. (1994). Nasal dosimetry modeling for humans. *Inhal. Toxicol.* **6(Suppl.),** 85–97.